

# Electronic Supplementary Information

## Nano-mechanical signature of brain tumours

Gabriele Ciasca, Tanya Enny Sassun, Eleonora Minelli, Manila Antonelli, Massimiliano Papi\*, Antonio Santoro, Felice Giangaspero, Roberto Delfini, Marco De Spirito

\*Corresponding author: massimiliano.papi@unicatt.it

### Corrugation of the sample and zero force images

In Fig. S1a-c, three representative Force-Distance (F-D) approach-retract cycles are reported. The maximum applied loading force was set to 5 nN. Indentation curves were analysed by using the Sneddon model, as detailed discussed in ref<sup>28,29,69-73</sup>.

$$F(\delta) = \frac{2E \tan(\alpha)}{\pi(1 - \nu^2)} \delta^2 \quad (1)$$

where E accounts for the apparent Young's modulus,  $\nu$  for the Poisson ration and  $\delta$  for the indentation depth. E is referred to as apparent Young's modulus to take into account the dependence of E on the scanner velocity and on the indentation depth. The Poisson ratio was set at 0.5 to account for material incompressibility.

Tissue topography was recovered directly in a liquid environment by mapping the tip contact-point retrieved from fitting eq.1 to experimental data, according to<sup>73</sup>. This procedure allowed us to acquire the zero-force image of the analysed tissues that minimizes shape modifications, e.g. height compression, induced by the applied force in conventional AFM imaging. Three representative zero-force 40  $\mu\text{m}$  x 40  $\mu\text{m}$  images of three investigated tissues are shown in Fig. S1d-f. Such images show that tissues are highly corrugated, with a peak to valley ratio of about 40  $\mu\text{m}$ .

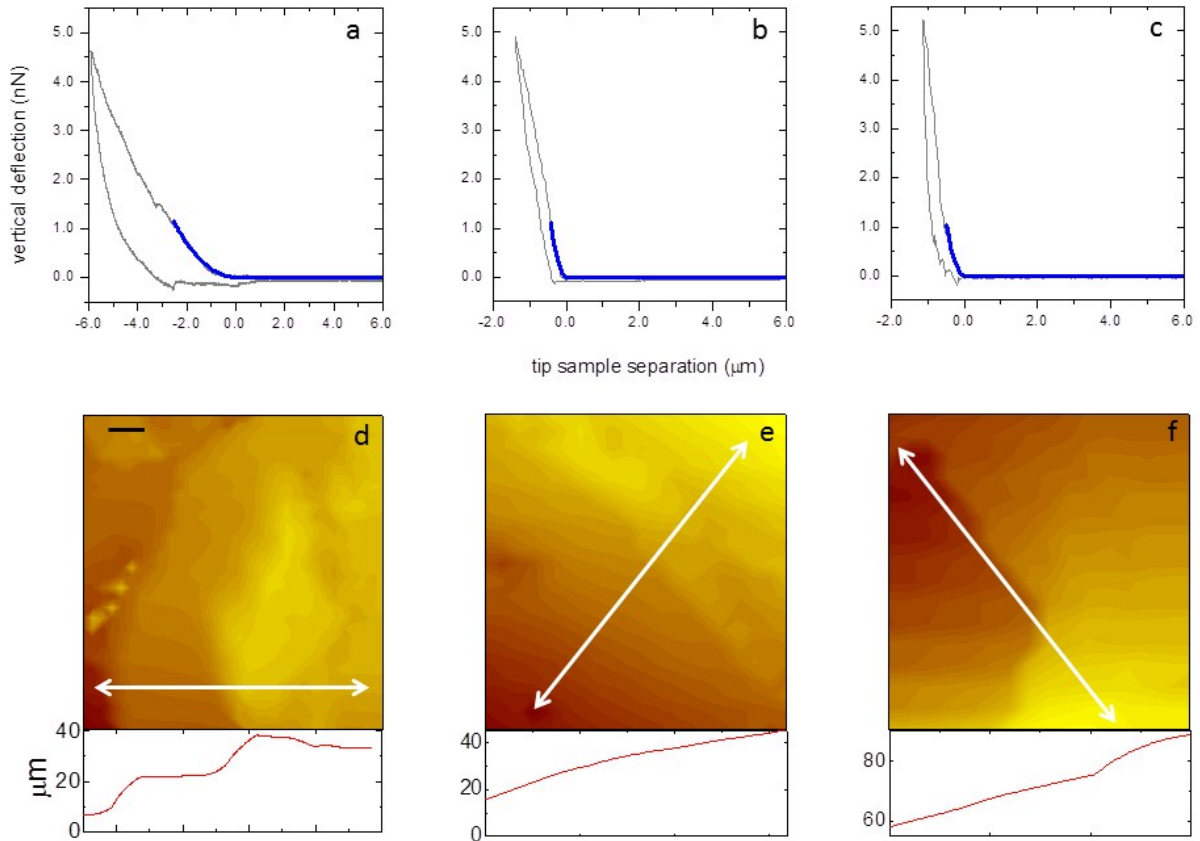


Figure S1: three representative indentation cycles acquired on a necrotic (a) and non-necrotic (b) GBM tissue, and on a meningioma tissue (c). Equation 1 was fitted to the approach curves to retrieve apparent Young's modulus and the tip-contact point (continuous blue line). Representative topological zero-force images (d-f) of the three analyzed samples (scale bar  $5\mu\text{m}$ ) with three line profiles (white arrows highlight the line selected to measure the corresponding profile).

### Effect of the use of different cantilevers on the measured E values.

Glioblastoma Multiforme (GBM) and Meningothelial meningioma (MM) have markedly different biomechanical properties. The latter, indeed, originates from meninges and thus can be extremely stiff. Therefore in the present paper we used two different commercial cantilevers provided by MicroMash, namely the CSC38 and CSC37 models, with different spring constant. CSC38 cantilevers were used to probe GBM tissues whereas CSC37 cantilevers were used to probe MM.

A comparison between the two different cantilevers in term of E is reported in fig S2, where we measured the same agar gel with two different cantilevers a with a spring constant encompassing the whole range adopted in our experiment.

Fig S2 demonstrate that measurements obtained with the two different models are consistent within the experimental error and in general the difference between the measured values is less than 10%.

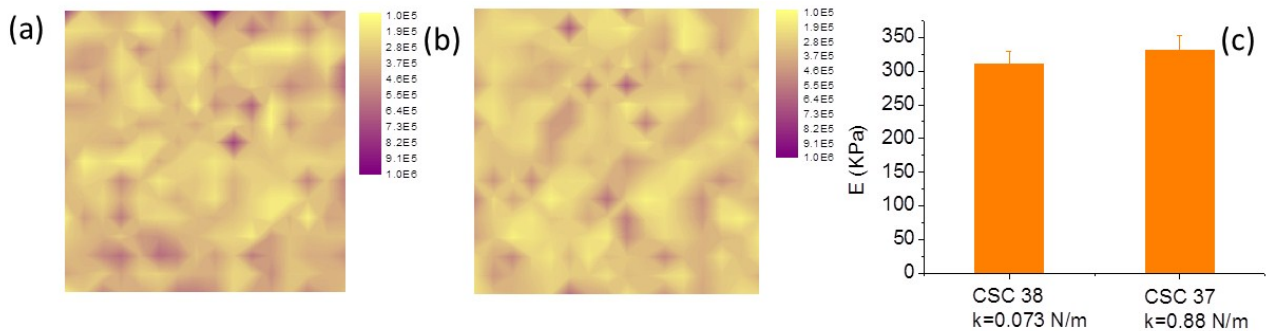


Figure S1: Two representative Young's Modulus maps acquired on an agar gel by using two different cantilevers with different spring constant, namely  $k=0.0730\pm 0.005$  N/m (a) and  $k=0.880\pm 0.007$  N/m (b). Bar plot of the mean  $\pm$  SEM of E calculated on both maps.

### Effect of the indentation depth in the determination of the apparent Young's Modulus E

In this work we chose to use sharp AFM probes in order to provide a nanoscale mapping of the mechanical properties of the analyzed tissues. When sharp probes are used, the retrieved E value is a function of the indentation depth and therefore E is usually referred to as apparent Young's modulus.

Such dependence does not compromise the comparison among different tissues because relative changes can be evaluated.

For the sake of completeness, we evaluated in fig. S3 the dependence of E on the indentation depth by using three representative force distance curves acquired on a GBM necrotic (S3 a), core (S3 b) and Meningioma (S3c) tissue.

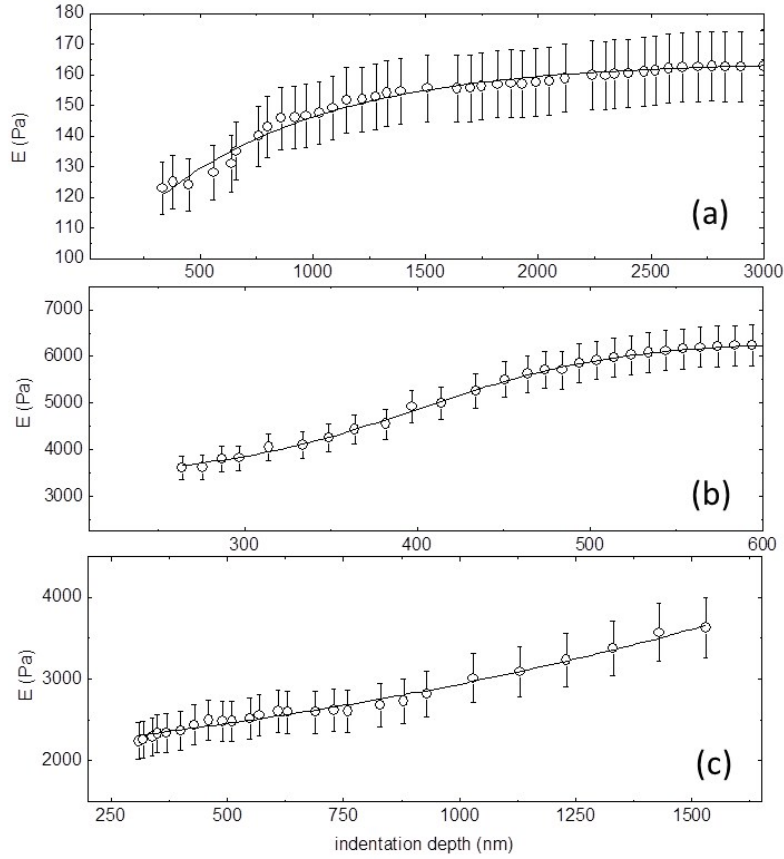


Figure S3: dependence of apparent Young's modulus E on the indentation depth evaluated by using three representative F-D curves acquired on a GBM necrotic (a), core (b) and Meningioma (c) tissue.

### Dependence of the E value on the particular choice of the contact point

The retrieved value of the apparent Young's modulus E is dependent on the particular choice of the contact point (CP). The determination of the statistical error on the CP and its effect on the E value is a controversial and very complicated issue.

We estimated both errors by using the statistical approach described in the following.

In the case of a nonlinear function of many parameters, the inverse of the covariance matrix (V) is related to the second derivative of the  $\chi^2$  function calculated its minimum ( $\hat{\theta}$ ):

$$(V^{-1})_{ij} = \frac{1}{2} \frac{d^2 \chi^2}{d\theta_i d\theta_j} \Big|_{\hat{\theta}}$$

This equation indicates that the covariance matrix depends only on the  $\chi^2$  curvature in its minimum. The previous equation allows for a simple determination of standard deviations ( $\sigma_i = \sqrt{V_{ii}}$ ). If one fixes all the variables except one, the previous equation assumes the simple form

$$\sigma^{-2} = \frac{1}{2} \frac{d^2 \chi}{d^2 \theta} \Big|_{\hat{\theta}}$$

In the minimum position the first derivative of  $\chi^2$  is zero and the function itself assumes the value  $\chi^2_{\min}$ . The following Taylor development can thus be obtained:

$$\chi^2(\theta \pm \sigma) = \chi^2(\theta) + \frac{1}{2} \frac{d^2\chi^2}{d\theta^2} \Big|_{\theta} \sigma^2 = \chi^2_{\min} + 1$$

Therefore we expect the  $\chi^2$  function has a parabolic behaviour in a small interval about its minimum. Most importantly, the standard deviation of the fit parameter (in our case, the contact point) can be evaluated in correspondence of the two values where the  $\chi^2$  function is increased by 1 (fig. S4). Practically, we used the JPK data processing software to find the best fit of F-D curves (more information on the fitting algorithm can be found here <http://www.nanophys.kth.se/nanophys/facilities/nfl/afm/jpk/manuf-manuals/DPmanual.4.2.pdf>).

Then we recorded the change in the fitted Young's modulus E and in the  $\chi^2$  by varying the contact point below and above the fitted value. As expected the larger the distance from the fitted value the larger the  $\chi^2$  function. In fig S3 a-c the behaviour of the  $\chi^2$  as a function of the contact point is shown for three different force distance curves with E values encompassing almost the whole range investigated. As expected, the  $\chi^2$  function has a parabolic behaviour in a small interval about its minimum for the three curves. Fig S4 shows that the larger the Young's modulus the smaller the  $\pm\sigma_{PC}$  interval about the expected value.

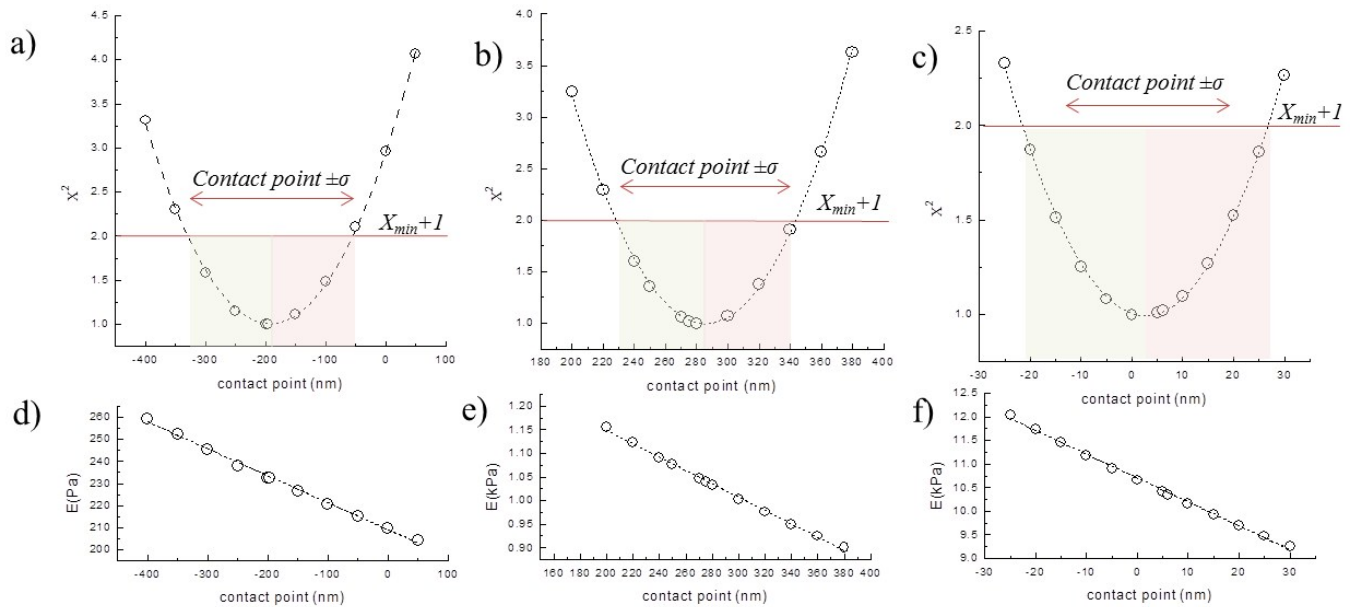


Figure S4: Behavior of the  $\chi^2$  function in an interval about the  $\chi^2$  minimum value. The standard deviation of the contact point is calculated in correspondence of the points where the  $\chi^2$  function is increased by 1. Curves were shifted for clarity.

It is well known that the analytical formula most-often used to estimate the error propagation is based on a first-order Taylor series expansion. As such, it makes the assumption that a small variation of, e.g., the contact point must propagate in a linear variation of the Young's modulus  $E$ . One can see that this assumption is fully verified in our case. Fig S3 shows indeed how a variation of the contact point within one  $\sigma$  reflects in a linear variation of the Young's modulus. This linear trend allows us to use the standard propagation formula to determine the statistical error of  $E$ . In particular the following

equation can be derived for the relative error of  $E$ ;  $\frac{dE}{E} = \frac{m\sigma_{CP}}{E}$  where  $dE = m\sigma_{CP}$  is the statistical error of  $E$  and  $m$  is the slope of the linear function. Such function allows us to determine a relative error of the order of 10% (7.7 % in fig d; 7.7 % in fig e and 11.8% in fig f).

### **height-dependent effect of the dual-resin epoxy glue on the sample mechanical properties.**

The mechanical characterization of tissue slices was carried in a liquid environment immediately after tumour resection without any further fixation process. This procedure was aimed to avoid any possible mechanical artefacts due to the sample preparation procedure. Typical tissues slice were 3-4 mm thick. In order to immobilize tissues on a petri dish we used an extremely thin layer of a fast drying biocompatible dual-resin epoxy glue according to the procedure developed in [30]. The dual resin epoxy glue was in contact with the bottom surface of the sample and, during the experiment, we indented the top-most surface, located approximately 3-4 mm far away from the glue layer.

To account for glue-induced modifications, we studied the dependence of the mechanical properties of the sample as a function of the distance from the glue layer. To this purpose, brain tissues were positioned as shown in the inset of fig. S5. Measurements were performed in a dry environment. This strategy allowed us to measure the sample without the need to fix it on the petri dish by using glue. This choice is justified because, as a matter of fact, tissues are placed in a liquid environment after the glue has dried and, thus, after that any diffusion process of the glue through the sample has stopped.

In fig. S5 we measured the sample stiffness as a function of the distance from the glue layer. A sigmoidal trend was fitted to data. Close to the glue layer, the sample appears to be extremely stiff, because of the glue. Then, sample stiffness decreases abruptly and reaches a

plateau at approximately 1 mm from the glue layer. For larger distance we do not measure any detectable variation of the sample stiffness showing the absence of a considerable amount of infiltrated glue. Even though we cannot categorically exclude the presence of small trace of glue, nevertheless we can state the mechanical measurements are not markedly affected by such infiltration, if any.

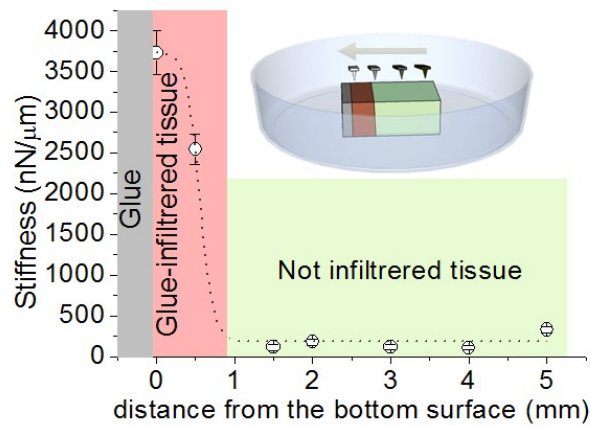


Figure S5: stiffness of a brain tissue slice as a function of the distance from the glue layer.